Catal Lett (2007) 118:165–172
DOI 10.1007/s10562-007-9196-4

Catalytic Removal of Toluene in Air over Co–Mn–Al Nano-oxides Synthesized by Hydrotalcite Route

Jean-François Lamonier · Aimé-Brice Boutoundou · Cédric Gennequin · Maria Josefina Pérez-Zurita · Stéphane Siffert · Antoine Aboukais

Received: 11 May 2007 / Accepted: 1 July 2007 / Published online: 25 July 2007

Abstract Co–Mn–Al hydrotalcite type solids were synthesized as precursors of catalysts for the total oxidation of toluene in air. For the as-prepared solids, XRD measurements indicate the coexistence of hydrotalcite and $MnCO_3$ phases. When calcination is performed at 500 °C, different mixed oxides are found as a function of Co:Mn molar ratio and preparation method, and very high specific surface areas were obtained for the Co–Mn solids. The comparison of catalytic activities in the presence of calcined hydrotalcites with those in the presence of calcined hydroxides evidences the superiority of the first oxides due to their higher reducibility. Co–Mn–Al nano-oxides synthesized using hydrotalcite type solids as precursors, are very promising candidates for the substitution of noble metal based solids.

Keywords Catalytic oxidation · VOC removal · Hydrotalcite precursors · Nano-oxides · Redox properties

1 Introduction

Volatile Organic Compounds (VOCs) are among the most common air pollutants emitted from chemical, petrochemical, and allied industries. VOCs are one of the main sources of photochemical reaction in the atmosphere leading to various environmental hazards. In France, since 1988, VOC emissions decreased around of 44% [1]. According to the Göteborg protocol, the maximum emission level should be of 1100 kt in 2010. In order to achieve the objective, different techniques such as absorption, catalytic oxidation and thermal incineration can be used. Catalytic oxidation is a promising process for VOCs elimination, since the reaction operates at temperatures much lower than those required for thermal incineration. The advantage of low oxidation temperature is the reduction of fuel consumption, particularly for large volumes of diluted VOC polluted air. Noble metal catalysts present higher activity than other metal catalysts, but their manufacturing cost is high. Therefore, efforts have been done to develop transition metal oxides with high catalytic activity. Among them, manganese or cobalt oxides are the most active phases for catalytic oxidation of VOCs [2–4] but these oxides usually present low specific surface area and poor thermal stability. An interesting way to obtain mixed oxides catalysts is through the use of hydrotalcites (HTs) or layered double hydroxides (LDHs) as precursors. Indeed after a calcination treatment mixed oxides are formed and possess unique properties like high surface area, good thermal stability, good mixed oxides homogeneity and basic properties [5]. The structure of hydrotalcites can be derived from a brucite structure ($Mg(OH)_2$) [5] in which part of the Mg^{2+} cations is substituted by a trivalent metal like Al^{3+}. Partial or total substitution of Mg^{2+} and Al^{3+} by, divalent cations ($M^{2+} = Zn^{2+}$, Ni^{2+}, Cu^{2+}, Co^{2+}, …) and trivalent cations ($M^{3+} = Fe^{3+}$, Cr^{3+}, …) respectively is possible, creating an excess of positive charges. These positive charges of the metal hydroxide layers is compensated by interstitial layers built of anions ($A^{m-} = CO_3^{2-}$,

J.-F. Lamonier (✉) · A.-B. Boutoundou · C. Gennequin · S. Siffert · A. Aboukais
Laboratoire de Catalyse et Environnement, EA 2598, Université du Littoral Côte d'Opale, Dunkerque 59140, France
e-mail: lamonier@univ-littoral.fr

M. J. Pérez-Zurita
Centro de Catálisis, Petróleo y Petroquímica, Escuela de Química, Facultad Ciencias, Universidad Central de Venezuela, Apartado, Caracas 47102, Venezuela

NO_3^-…) and water molecules. Subsequently, the general formula of a hydrotalcite like compound has the form: $[M^{2+}_{1-x}M^{3+}_x(OH)_2]^{x+}$ $(A^{m-})_{x/m} \cdot nH_2O$. These materials gain increasing importance as catalysts precursors for many reactions of industrial interest [6] like CH_4 and methanol reforming [7, 8], VOC oxidation [9, 10], hydrodesulfurization of Fluid Catalytic Cracking (FCC) gasoline [11], NO reduction [12] and removal of SO_2 and NO_x [13].

Among the metal oxides, manganese and cobalt oxides are very promising candidates for the catalytic removal of various VOCs. By example, Lahousse et al. [14] showed the good performance of γMnO_2 since this catalyst is much more active than Au/MnO_2 and Au/TiO_2 for the total oxidation of n hexane. Wyrwalski et al. [15] demonstrated that Co_3O_4 can be a very active phase for the toluene oxidation if this oxide is present in a nanometric scale. Since Cobalt and Manganese ions can reach variable oxidation states, the synthesis of mixed-oxide catalysts including Co and Mn elements seems very suitable for redox reactions and then for VOCs oxidation. Kovanda et al. [16] studied mixed oxides obtained from Magnesium containing hydrotalcites Co–Mg–Mn, Co–Mg–Al–Mn and Co–Mg–Al in the total oxidation of ethanol and N_2O decomposition. They reported that hydrotalcite synthesis was not successful in systems containing exclusively Co and Mn and stated that high (Co + Mn) content is essential for the total conversion of ethanol at lower temperature [16].

In the present study, Co/Mn/Al hydrotalcites have been investigated as precursors of VOCs oxidation catalysts. Co and Mn-rich mixed oxides have been studied with keeping the Al content unchanged in order to try to optimize their activity. To evaluate the pertinence of using hydrotalcites precursors, conventional mixed oxides has also been studied. The solids with several cationic compositions have been characterized before and after treatments under oxidizing atmosphere. Since it has been shown that the reducibility of cations:

(i) strongly depends on the stoechiometry of the catalysts obtained from HTs [5], and
(ii) can be partly associated with the catalytic performances towards VOC oxidation [17], experiments under reducing atmosphere were also performed on calcined samples.

Toluene has been chosen as a VOC probe molecule because monocyclic aromatic hydrocarbons are present in the industrial and automotive emissions [18] and because toluene presents an important Photochemical Ozone Creativity Potential (POCP = 63.7) [19].

2 Experimental Section

2.1 Preparation of Co–Mn–Al Hydrotalcites and Hydroxides and Corresponding Calcined Samples

Four samples were synthesized with different Co and Mn contents: $Co_{6-x}Mn_xAl_2HT$ with x = 0; 2; 4 and 6. The synthesis method was similar to that conventionally reported: a solution containing appropriate quantities of $Co(NO_3)_2{\cdot}6H_2O$ (FLUKA, >98%), $Mn(NO_3)_2{\cdot}4H_2O$ (LABOSI, >96%) and $Al(NO_3)_3{\cdot}9H_2O$ (FLUKA, >98%) was added slowly under vigorous stirring into NaOH (2 M) and Na_2CO_3 (1 M) aqueous solutions. The final pH was 9.5. The resulting slurry was heated at 60 °C for 24 h and the precipitate was filtered, washed several times with hot deionized water (7 × 200mL, 50 °C) and dried at 55 °C for 64 h. Conventional Co_6Al_2OH and Mn_6Al_2OH samples were also prepared by co-precipitation of nitrate elements with NaOH. The final pH was 9.5 and the precipitate was directly filtered, washed several times with hot deionized water (7 × 200 mL, 50 °C) and dried at 100 °C for 24 h. The calcination treatment was performed under a flow of air (4 L h^{-1}—2 °C min^{-1}—4 h at 500 °C); the solids obtained were named $Co_{6-x}Mn_xAl_2HT500$ (x = 0; 2; 4; 6), Co_6Al_2OH500 and Mn_6Al_2OH500.

2.2 Characterization Techniques and Methods

The specific surface area of solids was determined by the BET method at –196 °C using a Quantasorb Junior apparatus. Sample pretreatment was performed under flow conditions of pure N_2, at 80 °C or 120 °C (for dried or calcined solids respectively), for 30 min. The N_2 adsorption was operated using a nitrogen (30%) and helium (70%) mixture.

Differential Thermal and Thermogravimetric analyses (DTA/TG) (Netzsch STA 409 equipped with a microbalance) were conducted in a flow (75 mL min^{-1}) of air at a heating rate of 5 °C min^{-1} from room temperature to 1000 °C with a sample mass of about 30 mg.

Crystallinity of solids was determined at room temperature by X-Ray Diffraction (XRD) technique in a Bruker D8 Advance diffractometer equipped with a copper anode (λ = 1.5406 Å). The scattering intensities were measured over an angular range of $4° < 2\theta < 80°$ for all the samples with a step-size of $\Delta(2\theta) = 0.02°$ and a count time of 6 s per step. The diffraction patterns have been indexed by comparison with the "Joint Committee on Powder Diffraction Standards" (JCPDS) files. Crystallite size was determined using a graphics based profile analysis program (TOPAS from Bruker AXS) and the Scherrer method.

Temperature-Programmed Reduction (TPR) of the calcined catalysts was carried out in a conventional laboratory apparatus (Zeton Altamira AMI 200) consisting of a gas supply system with mass-flow controllers, a quartz U-reactor, a water vapor trap and a Thermal Conductivity Detector (TCD). Prior to the TPR experiments, ~30 mg samples were activated under argon at 150 °C for 1 h. The samples were then heated from ambient to 1000 °C under H_2 flow (5 vol. % in argon—30 mL min^{-1}) at a heating rate of 5 °C min^{-1}.

The activity of the catalysts (100 mg) was measured at atmospheric pressure in a continuous-flow U-glass reactor with internal diameter of 0.8 cm. Before each test, the catalyst was reactivated under a flow of air (industrial air from "Air products", 2 L h^{-1}) at 500 °C for 4 h. The flow of the reactant gases (1800 ppm of C_7H_8 in air) was adjusted (50 mL min^{-1}) by a Calibrage CAL PC–5 apparatus constituted of a saturator and one mass flow controller. After reaching a stable flow, reactants passed through the catalyst bed (VVH = 15300 h^{-1}) and the temperature was increased using an "Eurotherm" controller from ambient temperature to 500 °C (1 °C min^{-1}). The feed and the reactor outflow gases were analyzed on line by a micro-gas chromatograph (VARIAN CP4900) equipped with 2 columns (PPQ^HBF heated at 60 °C for CO and CO_2 separation and $52CB^H$ heated at 40 °C for toluene, benzene and water separation), each column being connected to a TCD.

3 Results and Discussion

3.1 Characterization of Non-calcined Hydrotalcites and Hydroxides Precursors

The XRD patterns of the HT precursors are reported in Fig. 1. The patterns clearly indicate the good crystalline order and the presence of the hydrotalcite phase (JCPDS 220700 for Co_6Al_2HT ((3) in Fig. 1)) and JCPDS 511526 for Mn_6Al_2HT (1) in Fig. 1))). These results are in good agreement with those reported by Perez-Ramirez [20], Kloprogge [21] and Aisawa [22]. When Mn is present, the coexistence of both $MnCO_3$ (JCPDS 441472 ((2) in Fig. 1))) and hydrotalcite phase is observed. Concentration of the $MnCO_3$ phase increases with increased Mn content.

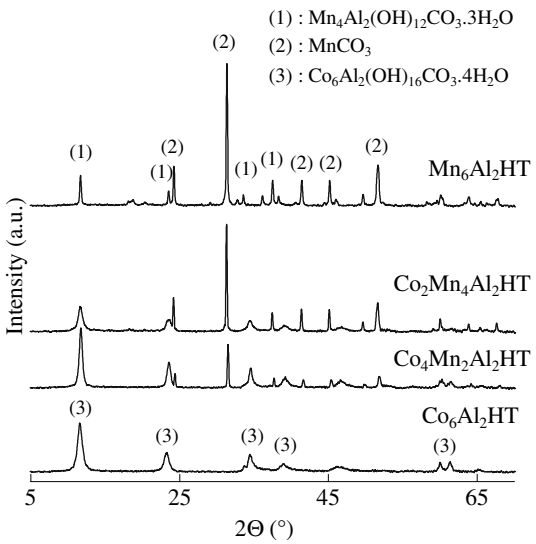

Fig. 1 XRD patterns of $Co_{6-x}Mn_xAl_2HT$ samples

The formation of manganese carbonate during the hydrotalcite synthesis has already been mentioned by Aisawa et al. [22]. In fact among all anions which can be used for the precipitation (Cl^-, CO_3^{2-}, NO_3^- and SO_4^{2-}), only the use of Cl^- and NO_3^- allows formation of Mn–Al hydrotalcite alone [22]. On the contrary, Kovanda et al. [16] found that synthesis of Co–Mn–Al hydrotalcites without $MnCO_3$ formation is possible even if an alkaline solution of Na_2CO_3 is employed during the preparation. This apparent discrepancy can be explained by the different M^{2+}(Co^{2+} and/or Mn^{2+})/Al^{3+} ratios used (ratio of 2 instead of 3). Indeed instead of forming the hydrotalcite type solid Mn_6Al_2HT, the solid $Mn_4Al_2(OH)_{12}{\cdot}3H_2O$ (JCPDS 511526) is obtained and subsequently Mn^{2+} species are available to react with carbonates to produce $MnCO_3$. The lattice parameters of the prepared HTs are listed in Table 1. The "a" lattice parameter decreases according to the decrease of M^{2+}/Al^{3+} ratio in $Co_4Mn_2Al_2HT$, due to the reaction between Mn^{2+} and CO_3^{2-}. Mn^{2+} oxidation into the upper oxidation state (Mn^{3+} and/or Mn^{4+}) is possible in our experimental conditions [23] and should confirm the decline of "a" lattice parameter, since radii of Mn^{3+} and Mn^{4+} ions are smaller than that of Co^{2+}. The small difference in "a" lattice parameter seems to indicate that only a part of Mn^{2+} species are oxidized in Mn^{3+} or Mn^{4+}.

XRD measurements were also performed on Co_6Al_2OH and Mn_6Al_2OH samples. As expected, the hydrotalcite phase is not formed. The XRD pattern of Co_6Al_2OH corresponds to $Co_5(O_{9.48}H_{8.52})NO_3$ (JCPDS 460605) while the XRD lines obtained for Mn_6Al_2OH have not been identified.

Table 1 shows the specific surface area values of the hydrotalcite type solids dried at 130 °C and calcined at 500 °C, the lattice parameters and the half width of (003) XRD peak. For $Co_{6-x}Mn_xAl_2HT$ samples dried at 130 °C, the specific surface area decreases with the decrease of the half widths of (003) XRD peak (2θ = 11.62°), indicative of a lower crystallinity of the hydrotalcite structure when Mn is present. This decrease can be also explained by the contribution of $MnCO_3$ phase (see XRD analysis) having a lower specific surface area. Besides, Mn_6Al_2OH synthesized in the absence of carbonates presents a higher specific surface area than that of Mn_6Al_2HT (Table 1).

The thermal decomposition (simultaneous DTA/TG analysis) behavior of HT and OH precursors is displayed in

Table 1 XRD parameters and specific surface areas values

Samples	Lattice parameters (Å)		Half width of (003) XRD peak (2θ in °)	Specific surface area ($m^2\ g^{-1}$)	Specific surface area ($m^2\ g^{-1}$)
	c	a		T = 130 °C	T = 500 °C
Co_6Al_2HT	22.875(9)	3.080(5)	0.77	111	121
$Co_4Mn_2Al_2HT$	22.614(0)	3.068(8)	0.50	66	187
$Co_2Mn_4Al_2HT$	22.674(4)	–	0.68	72	188
Mn_6Al_2HT	22.685(8)	–	0.25	45	115
Co_6Al_2OH	–	–	–	141	53
Mn_6Al_2OH	–	–	–	82	57

Fig. 2. The total weight loss of the samples is about 30–32 wt% except for the Mn_6Al_2OH solid (25 wt%). For the Co_6Al_2HT sample, two weight loss steps associated with two endothermic peaks are observed. The first endothermic peak (noted A) appears at 170 °C and corresponds to the loss of interlayer water, without collapse of the structure [20]. The second one (noted B) at higher temperatures (220 °C) is attributed to both dehydroxylation and decarbonation [20]. On the other hand, Kloprogge et al. [21] proposed that the decarbonation takes place during the first endothermic transition. As it is well known that Co–Al hydrotalcites decompose at lower temperatures than other hydrotalcites like Ni–Al where no collapsing of the layered structure is observed below 250 °C, the first explanation seems to be more accurate [24]. From the DTA curves (Fig. 2) it can be observed that the Mn substituted precursors are more thermally stable since the two decomposition peaks appear at higher temperatures than those observed for Co_6Al_2HT500. A third peak (noted C) is observed when Co is substituted by Mn. The proportion of C signal increases with Mn concentration in the solid. Then "C" peak can be attributed to the thermal decomposition of $MnCO_3$ into MnO_x. Besides, this peak is absent for $Mn_6Al_2(OH)$ according to the absence of $MnCO_3$ phase in this sample.

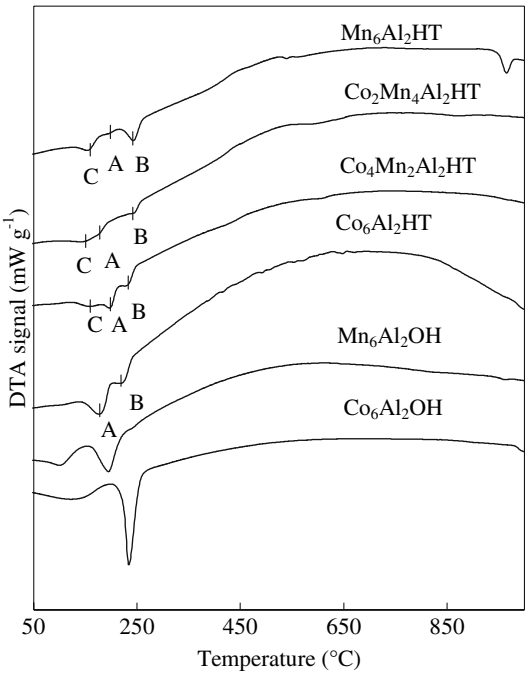

Fig. 2 DTA profiles obtained during the calcination of $Co_{6-x}Mn_xAl_2HT$, Co_6Al_2OH and Mn_6Al_2OH samples (5 °C min^{-1}, 75 mL min^{-1})

3.2 Characterization of Calcined Co–Mn–Al Hydrotalcites and Hydroxides

The calcination at 500 °C of "HT" samples leads to an enhancement of specific surface area values (Table 1). This increase is more pronounced for manganese containing solids. For the "OH" samples, the treatment at 500 °C leads to a significant decrease of the specific surface area. These different behaviors can be explained by the initial presence of the hydrotalcite phase. Indeed the hydrotalcites calcination leads first to the formation of amorphous compounds followed by pre-spinel oxides formation which can significantly contribute to increase the specific surface area [5]. Moreover, Reichle et al. [25] have earlier attributed this phenomenon to the pores/craters formation on the surface of the material through which water molecules and CO_2 escape (from interlayer) and showed that 60% of sample surface area is due to the contribution from these fine pores. Both explanations could explain our observed results.

XRD patterns of calcined Co–Mn–Al Hydrotalcites corroborate the observation made from the DTA/TG measurements and reveal the destruction of the HT phase (Fig. 3) and the mixed oxides formation (Table 2). Calcined Co_6Al_2 samples (HT or OH) give similar diffraction peaks. However for Co_6Al_2HT500 the diffraction peaks are broader according to the higher BET value of this sample (Table 1). The broadness of diffraction peaks can be also explained by the presence of a mixture of three

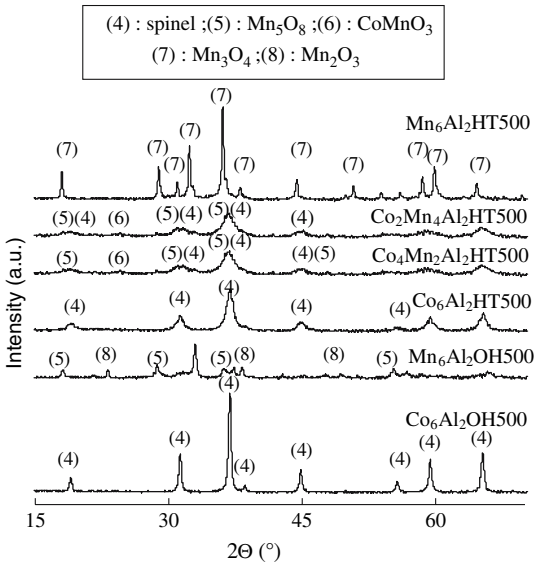

Fig. 3 XRD patterns of calcined $Co_{6-x}Mn_xAl_2HT500$, Co_6Al_2OH500 and Mn_6Al_2OH500 samples

oxide spinel phases very difficult to differentiate by XRD [26]: Co_3O_4 (JCPDS 421467), $CoAl_2O_4$ (JCPDS 440160) and Co_2AlO_4 (JCPDS 380814) (see (4) in Fig. 3 and Table 2). The formation of Co_3O_4 is due to the easy oxidation potential of Co^{2+} ions and the thermodynamic stability of Co_3O_4, higher than that of CoO in air [27]. The XRD patterns of $Co_{6-x}Mn_xAl_2HT500$ with x = 2 and 4 are also displayed in Fig. 3. The Co-oxide spinel quantity decreases with the rise of manganese content in the solid and the crystallize size of these species (Table 2) significantly decreases in agreement with the highest specific surface areas obtained for both solids. In addition to the oxide spinel phases, Mn_5O_8 and $CoMnO_3$ phases are produced (Table 2 and see respectively (5) and (6) in Fig. 3). Fritsch et al. [28] showed that Mn^{2+} and Mn^{3+} cations can be oxidized in the temperature range of 300–425 °C according to the following reaction:

$$Mn_3O_4 + 2/5\ O_2 \rightarrow 3/5\ Mn_5O_8.$$

Moreover for Co-free samples, XRD analysis emphasizes the importance of the preparation method to obtain manganese oxides since starting from hydrotalcite precursor, Mn_3O_4 structure is formed ((7) in Fig. 3) while starting from hydroxide precursor Mn_5O_8 and Mn_2O_3 ((5) and (8) respectively in Fig. 3) phases are produced. Apparently the stabilization of Mn^{2+} cations into hydrotalcite and $MnCO_3$ structures does not facilitate the oxidation of Mn_3O_4 into Mn_5O_8 at 500 °C.

TPR patterns of calcined samples are shown in Fig. 4. A general comment can be made concerning the effect of the preparation method: the reduction of mixed oxides synthesized via the hydrotalcite method is easier than that of mixed oxides conventionally prepared. When supported, smaller crystallites are usually more difficult to reduce due to a strong interaction of the species with the carrier. However the reduction of bulk oxides is easier even if the particle size of these species is rather small. The TPR results are in good agreement with XRD measurements which have demonstrated the formation of small crystallites of mixes oxides using hydrotalcite type solids as precursor. It is well established that the reduction is strongly influenced by the crystallite size. Reducibility of the solids prepared from a hydrotalcite precursor is better as the particle size is smaller (Table 2).

Based on the studies of Ribet et al. [29], the first peak observed for Co_6Al_2HT500 sample can be attributed to the reduction of Co_3O_4 into metallic Co whereas the second one to the reduction of $CoAl_2O_4$, these two spinel structures giving similar XRD patterns. In fact the first peak corresponds to reduction into two steps, $Co_3O_4 \rightarrow CoO \rightarrow Co$

Table 2 XRD identification of oxides present in calcined $Co_{6-x}Mn_xAl_2HT$ samples

Samples	Identified phases				
	Spinel(s)[a]	Mn_5O_8[b]	Mn_3O_4[c]	$CoMnO_3$[d]	Mn_2O_3[e]
Co_6Al_2HT500	■ (12)				
Co_6Al_2OH500	■ (39)				
$Co_4Mn_2Al_2HT500$	■ (7)	■ (41)		■ (nd)	
$Co_2Mn_4Al_2HT500$	■ (5)	■ (33)		■ (nd)	
Mn_6Al_2HT500			■ (39)		
Mn_6Al_2OH500		■ (18)			■ (47)

[a] Co_3O_4 (JCPDS 421467), $CoAl_2O_4$ (JCPDS 440160), Co_2AlO_4 (JCPDS 380814) or $MnCo_2O_4$ (JCPDS 320297)

[b] JCPDS 391218, [c]JCPDS 240734, [d]JCPDS 653696, [e]JCPDS 411442

Value in brackets corresponds to the crystallite size in nm

nd = "non-determined" due to the low content and crystallinity of this phase

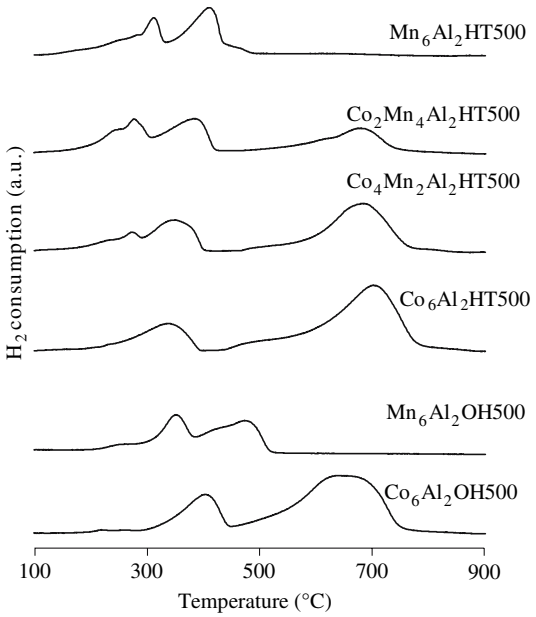

Fig. 4 H_2–TPR profiles of calcined $Co_{6-x}Mn_xAl_2HT500$, Co_6Al_2OH500 and Mn_6Al_2OH500 samples

which are almost indistinguishable [30, 31]. The polarization of Co–O bonds by Al^{3+} ions in $CoAl_2O_4$ compound induces an increase in reduction temperature of Co^{2+} species and explains well the presence of the second TPR peak. Since both peaks are also present for the H_2 consumption of Co_6Al_2OH500, Co_3O_4 and $CoAl_2O_4$ phases contribute to the mean crystallites size values calculated for Co_6Al_2HT500 and Co_6Al_2OH500 samples (Table 2).

The incorporation of Mn into the Co–Al system causes a modification of H_2-TPR profiles ($Co_4Mn_2Al_2HT(500)$ and $Co_2Mn_4Al_2HT(500)$). In fact the signal is the superposition of that obtained for Co_6Al_2 samples and one additional signal which can be attributed to the reduction of Mn_5O_8, $CoMnO_3$ and/or $MnCo_2O_4$ oxides identified or supposed by XRD measurements. Since Mn_5O_8 phase is also observed in Mn_6Al_2OH500, the TPR profiles of $Co_4Mn_2Al_2HT(500)$ and $Co_2Mn_4Al_2HT(500)$ catalysts have to be compared with that of Mn_6Al_2OH500. Bulk αMn_2O_3 shows two-step reduction: the first step can be attributed to the reduction of αMn_2O_3 into Mn_3O_4 (maximum at around 400 °C) whereas the second step can be assigned to the reduction of this Mn_3O_4 to MnO (maximum around 490 °C) [32, 33]. The H_2-TPR profile of Mn_6Al_2OH500 evidences the same two-step reduction between 380 °C and 525 °C according to the presence of Mn_2O_3 phase (Table 2). The peaks at lower temperatures observed for this sample can be then attributed to the reduction of Mn_5O_8. Consequently for $Co_4Mn_2Al_2HT(500)$ and $Co_2Mn_4Al_2HT(500)$ solids, the signal at low temperature can be assigned to the reduction of Co_3O_4 but also to the reduction of Mn_5O_8 species. The signal intensity at higher temperatures, signal previously attributed to reduction of Co ions included in a spinel structure, decreases with the decrease of the Co content in the sample.

The TPR profile of Mn_6Al_2HT500 is very different from that of Mn_6Al_2OH500 (Fig. 4), in agreement with the XRD results which have revealed different crystallographic structures. The pattern of this sample is much more complex and can not be attributed to the single reduction of Mn_3O_4 into MnO. Therefore it is suggested that reduction of amorphous compounds, formed after a calcination treatment at 500 °C (like manganese aluminates) but not detected by XRD, occurs.

The total amount of hydrogen consumed during reduction in the temperature range 100–800 °C decreases with the Mn incorporation in the sample (Table 3) according to the partial reduction of Mn oxides into MnO and the complete reduction of Co oxides into metallic Co in the same temperature range.

3.3 Catalytic Activity of Calcined Co–Mn–Al Hydrotalcites and Hydroxides

The samples calcined at 500 °C were tested as catalysts in the total oxidation of toluene (Fig. 5). When the toluene conversion is complete, H_2O and CO_2 are the only products observed. However when conversion is incomplete, benzene is produced. Around 50 ppm of benzene are formed during the catalytic test. Since the initial concentration of toluene is of 1800 ppm, the quantity of benzene formed is very low. Maximum benzene production is observed in the temperature range of 240–350 °C depending on the catalyst used and the toluene conversion. The formation of benzene during the oxidation of toluene has already been observed over rhodium-based catalysts [34]. In the catalytic oxidation of toluene different reaction paths have been already recognized [35]. The most important reaction path is the one initiated by attack on the methyl group with subsequent oxidation steps [36]. However the direct dealkylation of toluene into benzene is plausible [36] considering the detection of others products which can be "cracking" products as ethylene and pentadiene.

Table 3 H_2-TPR quantitative results and temperatures measured at 50% of toluene oxidation (T_{50}) for the calcined samples

Samples	H_2 consumption (μmol H_2 g^{-1})		T_{50} (°C)
	(100–800 °C)	(up to 400 °C)	
Co_6Al_2HT500	11423	2400	287
$Co_4Mn_2Al_2HT500$	10064	3563	267
$Co_2Mn_4Al_2HT500$	8307	4382	247
Mn_6Al_2HT500	5093	4337	249
Co_6Al_2OH500	12091	2844	343
Mn_6Al_2OH500	5256	2132	291

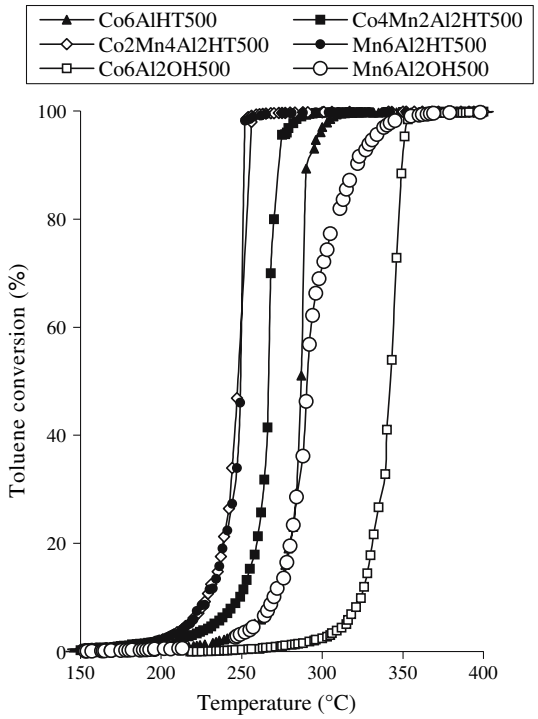

Fig. 5 Conversion of toluene (%) on $Co_{6-x}Mn_xAl_2HT500$, Co_6Al_2OH500 and Mn_6Al_2OH500 catalysts vs reaction temperature (°C)

The T_{50} temperature, at which 50% toluene conversion was achieved, was chosen as a measure of catalytic activity of the mixed oxides (Table 3). The catalytic activity order can be established as: $Co_2Mn_4Al_2HT(500) = Mn_6Al_2HT(500) > Co_4Mn_2Al_2HT(500) > Co_6Al_2HT(500) = Mn_6Al_2OH(500) >> Co_6Al_2OH(500)$.

The results evidence some correlations between T_{50} values and (i) surface area (ii) mixed oxides composition and (iii) mixed oxides reducibility.

$Co_6Al_2(500)$ and $Mn_6Al_2(500)$ samples are much more active in the toluene oxidation when catalyst is synthesized starting from hydrotalcite phase. These catalytic results can be correlated directly with the highest specific surface area values obtained for "HT" calcined samples (Table 1). The difference of activity between $Mn_6Al_2HT(500)$ and $Mn_6Al_2OH(500)$ can also be explained by the produced manganese oxide form, which significantly influences the catalytic performances in VOC oxidation. Indeed γ MnO_2 [37] and Mn_3O_4 [3] are reported to be very efficient phases for VOC oxidation. Baldi et al. [38] showed that α Mn_2O_3 is however less active than Mn_3O_4 for both propane and propene oxidation. This result is in good agreement with our catalytic measurements observed in the presence of $Mn_6Al_2HT(500)$ (Mn_3O_4) and $Mn_6Al_2OH(500)$ (Mn_5O_8 + Mn_2O_3) samples.

When comparing "HT samples" amongst themselves, it seems that high Mn contents in the catalyst are desired for toluene oxidation. However the partial substitution of Mn by Co giving $Co_2Mn_4Al_2HT(500)$ catalyst led to identical catalytic activity (Fig. 5 and Table 3). This result can be partly explained by the high specific surface area of this solid since despite their similar specific surface area values and bulk compositions, $Co_2Mn_4Al_2HT(500)$ and $Co_4Mn_2Al_2HT(500)$ samples have very different catalytic behavior (T_{50} increased of about 20 °C in the presence of the second catalyst).

The comparison of H_2-TPR profiles revealed that the reduction of mixed oxides starts at lower temperature for "HT" samples than for "OH" samples. Therefore easier reducibility can also explain the best catalytic results obtained in the presence of calcined "HT" samples for the toluene oxidation in comparison with those observed in the presence of calcined "OH" solids. In order to clarify the catalytic results, the amount of hydrogen consumed during the reduction of calcined HT samples in the temperature range of catalytic activity (up to 400 °C) have been evaluated from the H_2-TPR measurements (Table 3). It is remarkable to note that the reducibility of mixed oxides rules the catalytic activity. Indeed a direct relationship between the reducibility of the mixed oxides species and their reactivity in the toluene oxidation is observed. $Mn_6Al_2HT(500)$ and $Co_2Mn_4Al_2HT(500)$ samples consumed the same amount of hydrogen and have the same catalytic activity.

This result lead us to the conclusion that toluene catalytic oxidation on Co–Mn–Al oxides takes place most likely via a redox mechanism in which the rate determining step would be the oxygen removal of the metal oxide to oxidize toluene. Easier but also higher extend of reduction of mixed oxides present in $Mn_6Al_2HT(500)$ and $Co_2Mn_4Al_2HT(500)$ samples lead to an efficient catalyst for catalytic toluene removal. Studying the activation process over Pd perovskite-type oxides, Giraudon et al. [39] have shown that, in the same test conditions, toluene is fully oxidized at 225, 250 and 280 °C over respectively Pd(0.5 wt%)/$LaFeO_3$, Pd(0.5 wt%)/$LaCoO_3$ and Pd(0.5 wt%)/$LaNiO_3$ catalysts. Since in our study a temperature of 250 °C is needed to completely convert toluene into CO_2 and H_2O over $Co_2Mn_4Al_2HT(500)$ and $Mn_6Al_2HT(500)$ samples, we can stated that Co–Mn–Al nano-oxides synthesized by hydrotalcite route are very promising candidates for the substitution of noble metal based solids.

4 Conclusions

In this study, Co–Mn–Al hydrotalcites with different compositions were prepared by a coprecipitation method. The formation of manganese carbonate during the hydrotalcite synthesis was observed for all Mn containing solids. The thermal decomposition at 500 °C leads to

mixed Co–Mn oxides with high specific surface areas (>180 $m^2\ g^{-1}$). Higher activity for toluene oxidation is observed in the presence of Mn-rich samples especially for $Co_2Mn_4Al_2HT(500)$. This was explained by the highest reducibility of this solid, which contains in fact a mixing of nano-crystallites of Co-spinel, Mn_5O_8 and $CoMnO_3$ phases. Indeed catalytic measurements and TPR results suggest that the redox properties of the catalysts play important role in the total oxidation reaction of the toluene. The use of hydrotalcite type solids as precursors of Co–Mn–Al mixed oxide catalysts seems to be an excellent alternative to noble metal catalysts for the total oxidation of toluene.

Acknowledgment This work was supported by the "Région Nord—Pas de Calais" through a research grant and the IRENI program.

References

1. Serveau L (2005) CITEPA report February 2005, 26
2. Lamaita L, Peluso MA, Sambeth JE, Thomas HJ (2005) Appl Catal B: Env 61:114
3. Baldi M, Finocchio E, Milella F, Busca G (1998) Appl Catal B: Env 16:43
4. Ataloglou T, Vakros J, Bourikas K, Fountzoula C, Kordulis C, Lycourghiotis A (2005) Appl Catal B: Env 57:299
5. Cavani F, Trifiro F, Vaccari A (1991) Catal Today 11:173
6. Vaccari A (1999) Appl Clay Sci 14:161
7. Yong ST, Hidajat K, Kawi S (2004) J Power Sources 91:131
8. Takehira K, Shishido T, Shoro D, Murakami K, Honda M, Kawabata T, Takaki K (2004) Catal Commun 5:209
9. Alejandre A, Medina F, Rodriguez X, Salagre P, Sueiras JE (1999) J Catal 188:311
10. Bahranowski K, Bielanska E, Janik R, Machej T, Serwicka EM (1999) Clay Miner 34:67
11. Zhao R, Yin C, Zhao H, Lin C (2003) Synthesis, Fuel Proces Technol 81:201
12. Kannan S (1998) Appl Clay Sci 13:347
13. Palomares AE, Lopez-Nieto JM, Lazaro FJ, Lopez A, Corma A (1999) Appl Catal B: Env 20:257
14. Cellier C, Lambert S, Gaigneaux EM, Poleunis C, Ruaux V, Eloy P, Lahousse C, Bertrand P, Pirard J-P, Grange P (2007) Appl Catal B: Env 70:406
15. Wyrwalski F, Lamonier J-F, Perez-Zurita MJ, Siffert S, Aboukaïs A (2006) Cat Lett 108:87
16. Kovanda F, Rojka T, Dobesova J, Machovic V, Bezdicka P, Obalova L, Jiratova K, Grygar T (2006) J Solid State Chem 179:812
17. Wyrwalski F, Lamonier J-F, Siffert S, Aboukaïs A (2007) Appl Catal B: Env 70:393
18. Chien CC, Chuang WP, Huang TJ (1995) Appl Catal A: Gen 131:73
19. Derwent RG, Jenkin ME, Saunders SM, Pilling MJ (1998) Atmos Environ 32:2429
20. Pérez -Ramirez J, Mul G, Moulijn JA (2001) Vib Spectrosc 27:78
21. Theo Kloprogge J, Frost RL (1999) Appl Catal A: General 184:64
22. Aisawa A, Hirahara H, Uchiyama H, Takahashi S, Narita E (2002) J Solid State Chem 167:152
23. Rey F, Fornés V, Rojo, J.M (1992) J Chem Soc Faraday Trans 88:2233
24. Millange F, Walton RI, D. O'Hare (2000) J Mater Chem 10:1713
25. Reichle WT, Kang SY, Everhardt DS (1986) J Catal 101:352
26. Pérez-Ramirez J, Mul G, Kapteijn F, Moulijn JA (2001) Mater Res Bull 36:1769
27. Sato T, Fujita U, Endo T, Shimada M, Tsunashima A (1988) React Solids 5:219
28. Fritsch S, Sarrias J, Rousset A, Kulkarni GU (1998) Mater Res Bull 33(8):1185
29. Ribet S, Tichit D, Coq B, Ducourant B, Morato F (1999) J Solid State Chem 142:382
30. Arnoldy P, Moulijn JA (1985) J Catal 93:38
31. Sexton BA, Hughes AE (1986) J Catal 97:390
32. Döbber D, Kieβling D, Schmitz W, Wendt G (2004) Appl Catal B: Env 52:135
33. Koh DJ, Chung JS, Kim YG, Lee JS, Nam IS, Moon SH (1992) J Catal 138:630
34. Patterson MJ, Angove DE, Cant NW, Nelson PF (1999) Appl Catal B: Env 20:123
35. Germain J-E, Laugier R (1971) Bull Soc Chim Fr 2:650
36. Lars S, Andersson T (1986) J Catal 98:138
37. Peluso M, Sambeth J, Thomas H (2003) React Kinet Catal Lett 80:241
38. Baldi M, Escribano VS, Amores JMG, Milella F, Busca G (1998) Appl Catal B: Env 17:L175
39. Giraudon J-M, Elhachimi A, Wyrwalski F, Siffert S, Aboukaïs A, Lamonier J-F, Leclercq G (2007) Appl Catal B: Env in press